Title

DFT investigations for the catalytic reaction mechanism of methane combustion occurring on Pd(ii)/Al-MCM-41

Journal

Physical Chemistry Chemical Physics, 20(39)

ISSN

0956-5000

Authors

Gannouni, Anis
Michel, Carine
Delbecq, Françoise
et al.

Publication Date

2018-10-10

DOI

10.1039/c8cp04178d

Peer reviewed

DFT investigations for the catalytic reaction mechanism of methane combustion occurring on Pd(II)/Al-MCM-41

Anis Gannouni[a], Carine Michel[b] , Françoise Delbecq[b], Mongia Saïd Zina[a], Philippe Sautet*[b,c,d]

[a] Université de Tunis El Manar, Faculté des Sciences de Tunis, Laboratoire de Chimie des Matériaux et Catalyse, Campus Universitaire, Tunis 2092, Tunisie.
[b] Univ Lyon, Ens de Lyon, CNRS UMR 5182, Université Claude Bernard Lyon 1, Laboratoire de Chimie, F69342, Lyon, France.
[c] Department of Chemical and Biomolecular Engineering, University of California Los Angeles, Los Angeles, CA 90095, United States
[d] Department of Chemistry and Biochemistry, University of California Los Angeles, Los Angeles, CA 90095, United States

Abstract :

In this work, a theoretical analysis was carried out on the mechanism of methane combustion occurring on the single site palladium oxide species $[Pd]^{2+}$ supported on a Al-MCM-41 silica. Single sites Pd-Oxo and PdO_2-Superoxo structures were used to represent the active centers. Activation energies for all the elementary steps involved in the oxidation of methane into formaldehyde are presented. The competition of methane / methanol substrates on active sites was examined. It was found that the formation of methanol via the reaction of methane with the superoxo species, formed via the adsorption of O_2 on reduced Pd (II) centers, facilitates the production of the very active Pd-Oxo catalytic sites.

1. Introduction

The catalytic combustion of methane has received much attention in the last decade due to its increasing application in environment-friendly fuel combustion with reduced emission of nitrogen oxides.[1-4] Catalysis is an effective way to augment the combustion. However, its efficiency is related to the ability to initiate the oxidation cleaving the strong C-H bond in CH_4 at temperatures as low as possible, with a typical temperature range of 300°-500°C. Two kinds of catalysts have been mainly used for methane combustion, the most popular supported noble metals such as Pd, Pt and Rh[5,6], and the common transition metal oxides or mixed metal oxides as bulk or supported catalysts.[7] Recently, supported palladium showed a good activity in this catalytic combustion process and a good thermal stability,[7-14] in particular, much attention has been paid recently to palladium supported on acid silica-alumina amorphous mesoporous supports, such as Al-MCM-41, H-ZSM-5 or SBA-15,[8,12,14] which shown good performances at temperature as low as 320°C using a fixed-bed reactor at atmospheric pressure and a feed gas with 1 vol % CH_4 and 20 vol % O_2.[15]

The performance of such solid catalysts is related to the metal oxidation state, the dispersion, and the morphology of the particles that depend on the precursors, the preparation route and the nature of the support, which complicates the characterization efforts to elucidate the nature of the active site. In the case of the Pd supported on silica-alumina mesoporous supports, the nature of the active site was debated in the literature in the past decade. Several studies identified nanoparticules of PdO,[5,13] while other proposed a PdO_2 phase, but for other oxidative processes such as the oxidative carbonylation of methanol[16] and the CO oxidation.[17] According to our previous works on Pd/Al-MCM-41,[8,18] CH_4 combustion could be due not only to nanoparticles of PdO but also to isolated Pd^{2+} cations which are coordinated by the oxygen atoms of the alumino-silicate framework and can be oxidized into palladium oxo species $[Pd=O]^{2+}$. The importance of isolated PdO_x species was also proposed on H-ZSM-5 in a Pd-based catalyst that could completely catalyze CH_4 to CO_2 at temperature as low as 320 °C.[15] Those experimental works were also strongly supported by theoretical studies of CH_4 oxidation, mainly by means of Density Functional Theory (DFT).[15,18,19] In particular, the pivotal role of the acid sites was evidenced for the activation of CH_4 and dispersion of isolated $[Pd=O]^{2+}$. Those sites act as anchoring sites for isolated Pd atoms in the alumino-silica framework, tuning the acido-basicity of the Pd^{2+} cation and its oxidized form, $[Pd=O]^{2+}$. In addition, the oxygen atoms of the support framework are involved in the early stages of the methane combustion, namely the formation of CH_3OH. Focusing mainly on the C-H

activation in methane by anchored isolated $[Pd=O]^{2+}$ species, those studies have not addressed the key issue of the generation and regeneration of the postulated active site. The oxidation of methane into methanol by $[Pd=O]^{2+}$ leaves a reduced Pd^{2+} center that cannot be active to further oxidize methanol into formaldehyde and then CO_2. And the generation of $[Pd=O]^{2+}$ from Pd^{2+} and O_2 remains a critical opened question in the case of isolated sites. To clarify the viability of the single sites hypothesis, further studies on the underlying mechanism in methane combustion are clearly necessary. Provided the experimental difficulties at distinguishing isolated $[Pd=O]^{2+}$ from PdO nanoparticles whom formation can't be easily avoided, DFT investigations of the catalytic activity are essential.

On earlier transition metals, several studies addressed those issues in a variety of oxidative processes using O_2 as a oxidant. For instance, in their theoretical study of the oxidation of CH_4 to CH_2O catalyzed by isolated silica-supported molybdate species, Bell et al.[20] have found that the process starts with the adsorption of O_2 on reduced Mo^{IV} centers generating peroxide species that are active in methane oxidation. Additionally, Fellah et al.[21,22] have comprehensively studied the oxidation of methanol to formaldehyde by oxo [M-O] and dioxo [O-M-O] species in ZSM-5 zeolite (M : Fe and V), formed from decomposition of N_2O on [M] and [M–O], respectively. Additionally, Liang et al.[23] have investigated methane oxidation to methanol with di-oxygen species in a Fe exchanged zeolite. Ona et al. [24] studied the energetics for direct methane oxidation to methanol on Fe- and Co-ZSM-5 clusters with mononuclear metal sites and the water effect on methanol formation. In these last studies [20-22] is was found that iron-dioxo species and di-oxo molybdate species (MO_2, M : Fe and Mo), react with methane to give formaldehyde. Those studies suggest an activation of the di-oxygen molecule by isolated early transition metal centers. As a late transition metal, this route may not be viable. In this article, we investigate the generation of the $[Pd=O]^{2+}$ species via the di-oxo but also the peroxo and superoxo intermediates using a model of Pd/Al-MCM-41 zeolite. We also complete the mechanistic investigation of the methane combustion. This oxidative process consumes two oxygen molecules. We focus here on the activation and consumption of the first oxygen molecule to oxidize methane into formaldehyde, since the further oxidation of formaldehyde into CO_2 is known to be much easier.

2. Computational models and methodology

2.1. Theoretical Models

In our previous studies on the site occupancy for palladium oxidation states in mesoporous Al-MCM-41 materials [25] it has been suggested by the analysis of FTIR and Raman spectra coupled with the calculated reaction energies that Pd^{2+} preferred sites contained in 6- or 8-membered rings. Furthermore we have also investigated the direct conversion of methane to ethanol by PdO/Al-MCM-41 and found that the $[Pd=O]^{2+}$ species supported on a 8-membered ring was more reactive than those supported on a 6-membered ring.[18] For this reason, we limit ourselves in the present work to location of the Pd^{2+} cation on a 8-membered ring. We have represented the surface of acid silica-alumina using structures of silsesquioxane type that simulate the 8 membered rings in which two Si atoms were substituted by two Al atoms ($(H_{18}Al_2Si_{14}O_{24})$, see **Figure S1**). The termination of these clusters was achieved by H-Si≡ groups instead of H-O-Si≡ groups, in order to avoid additional intramolecular hydrogen bonds and unrealistic physico-chemical properties.[26-29] The Pd^{2+} species supported on silica Al-MCM-41 reads Pd•MS with MS= $H_{16}Al_2Si_{14}O_{24}$ for a correct charge balance and is designated by **≡Pd**, while the $[PdO]^{2+}$ species is designated by **≡Pd(O)**. After O_2 being adsorbed on (Pd•MS), three configurations of the O and Pd atoms were considered based on previous quantum chemical studies [16,17,30,31] showing that cationic $[PdO_2]^{2+}$ are stable as $(Pd\text{-}O\text{-}O)^{2+}$, a superoxo species, $(O\text{-}Pd\text{-}O)^{2+}$, a dioxo species, and $(Pd(O_2)^{2+})$, a peroxo species. In the following, these complexes will be more simply denoted **≡Pd(O$_2$)$_{Peroxo}$**, **≡Pd(O$_2$)$_{Superoxo}$** and **≡Pd(O2)$_{Dioxo}$**. **Figure 1** shows the structures of the clusters.

2.2. Methods

All calculations were performed using the Gaussian 09 program[32] within density functional theory (DFT) using the OPBE[33] functionals that has already proven a reasonable accuracy for the electronic structure, which concurs with available experimental observations[34] and catalytic reactivity.[35,18] Unrestricted DFT was used for all calculations of the singlet and triplet PES. The triple-ζ plus polarization basis set (TZVP)[36] was used for the following atoms: silicon, oxygen, aluminum and hydrogen. For palladium, the pseudopotential of Hay and Wadt has been used together with the LANL2TZ basis sets as implemented in the code. The $[PdO_2]^{2+}$ species bonded to silica were treated as free-standing molecules. The optimized structures were characterized by frequency calculations, and all energies provided later include the zero-point vibrational energies unless otherwise stated. The Gibbs free energies of reactions are not discussed but they are reported in supplementary material using a standard state for all species present in the gas phase to 1 atm and a temperature of 773 K (Table S1). The major differences with the ZPE corrected energies lie in the adsorption and desorption

steps of the gas molecules on the active site embedded in the Al-MCM-41 mesoporous solid. Including properly those effects is beyond our model and it is not expected to modify the mechanism feasibility. Transition-state structures (TS) on the potential energy surface were located using the synchronous transit-guided quasi-Newton method. All TS were verified by the presence of a single imaginary frequency corresponding to the reaction coordinate to ensure that the TS led to the reactants and products of interest. In addition to visualization of the imaginary vibrational mode, the intrinsic reaction coordinate (IRC) was followed in both directions. The atomic charges were calculated using the approach proposed by Mulliken.[37]

3. Results

3.1 Geometric structure and electronic and bonding characteristics of the $\equiv Pd(O_2)_{Peroxo}$, $\equiv Pd(O_2)_{Superoxo}$ and $\equiv Pd(O_2)_{Dioxo}$ clusters.

The oxidized form of palladium PdO_2 deposited on aluminosilicate 8-MR is obtained according to equation (1)

$$\equiv Pd + O_2 \rightarrow \equiv Pd(O_2) \quad (1)$$

The electronic formation energy in gas phase of the three species (peroxo, superoxo and dioxo) was calculated at the UOPBE level as shown in **Table S2**. The optimized structures of $\equiv Pd(O_2)_{Peroxo(t)}$, $\equiv Pd(O_2)_{Superoxo}$ and $\equiv Pd(O_2)_{Dioxo(t)}$ were obtained taking the total charge as neutral and considering either singlet (s) or triplet (t) ground states. It has been shown previously[18] that for the C−H bond cleavage by an oxo Pd^{IV}=O species supported on silica Al-MCM-41, the transition state for the quintet state is far too high compared to the singlet and triplet states, which eliminates this spin state as a plausible pathway. Furthermore, the quintet state could not be localized in the case of the superoxo specie. Hence only the singlet and triplet PES described in the following. The corresponding structures are displayed in **Figure 1**. The most stable state is the singlet for [≡Pd] and the triplet for [≡Pd(O)].[18,25] The singlet state could not be localized in the case of the dioxo and peroxo species, thus the triplet sate has been considered as the ground state. The formation energy of $\equiv Pd(O_2)_{Superoxo(t)}$ in the triplet state is found more favorable than in the singlet state (compare $\equiv Pd(O_2)_{Superoxo(t)}$ and $\equiv Pd(O_2)_{Superoxo(s)}$, ΔE= -24 kJ/mol, **Table S2**) which is in agreement with the theoretical work of Ma and coworkers [16] on the PdO_2-Superoxo species located on a 6-membered ring β zeolite.

The comparison of those various systems indicates that the formation of the superoxo species by adsorption of molecular O_2 on the ≡Pd is the most favorable with an exothermic formation

energy (ΔE = -10 kJ/mol, **Table S2**). This greater stability can be related to the larger number of bonds with the aluminosilicate framework. Indeed, in $[\equiv Pd(O_2)]^{2+}$ peroxo and superoxo, the Pd atom always interacts with four oxygen atoms (see **Figure 1**), but the Pd atom is out of the ring plane in the dioxo and peroxo complexes with only two Pd-O bonds with the basic O of the alumino-silicate framework, while it is in the plane in the superoxo species with three Pd-O bonds to the framework. As shown in our previous studies,[18,25] the larger the numbers of basic oxygen atoms interacting with Pd(IV), the more stable the corresponding structure.

The high instability of the dioxo species compared to the others may be related to the oxidation of the Pd center from +IV to +VI upon O_2 dissociation (O1-O2 distance of 275pm). This instability implies that the O_2 molecule is not activated on ≡Pd and that the direct decomposition of O_2 is impossible. Additional support can be found from the Mulliken atomic charges for dioxo on the atoms O1 and O2 (structures with label are shown in **Figure 1**, charges are reported in **Table S3**). Last, the O-O distance is barely modified upon adsorption on ≡Pd in the superoxo and peroxo species: the O-O distance is 121pm and 126 pm in the superoxo and peroxo respectively to be compared with 121 pm in isolated O_2.

3.2 Oxidation of methane to methanol on the ≡Pd(O_2) cluster

Since the Pd dioxo $\equiv Pd(O_2)_{Dioxo(t)}$ is very unstable, we limited our study of the C–H bond activation of methane to the $\equiv Pd(O_2)_{Peroxo(t)}$, $\equiv Pd(O_2)_{Superoxo(t)}$ and $\equiv Pd(O_2)_{Superoxo(s)}$ clusters. The approach of methane to these clusters leads to $\equiv Pd(O_2)(CH_4)$ (**Figure S2**) according to the reaction (Eq 2),

$$\equiv Pd(O_2) + CH_4 \rightarrow \equiv Pd(O_2)(CH_4) \qquad (2)$$

followed by the oxidation of methane to methanol according to reaction (Eq 3).

$$\equiv Pd(O_2)(CH_4) \rightarrow \equiv Pd(O)(CH_3OH) \qquad (3)$$

The energy profiles for the different clusters at the various spin states are given in **Figure 2**. On $\equiv Pd(O2)_{Superoxo(t)}$, the reaction proceeds in two steps. First, the H atom abstraction to form the methyl radical leads to the intermediate labeled $\equiv Pd(OOH)(CH_3)$, via the transition state $TS_{1\text{-}Superoxo}(t)$ with an activation energy of 151 kJ/mol. The second step is the methyl migration via $TS_{2\text{-}Superoxo}(t)$ to form the methanol product with an activation energy of 60 kJ/mol. In the final state $\equiv Pd(O)(CH_3OH)$, methanol is bound to the oxo oxygen atom, by a hydrogen bond as a ligand forming a loose complex (**Figure S2**). In the case of $\equiv Pd(O_2)_{Peroxo(t)}$ and of $\equiv Pd(O_2)_{Superoxo(s)}$, the intermediate $\equiv Pd(OOH)(CH_3)$ does not exist and the final state is

obtained directly from TS_1 with activation energies of 262 and 169 kJ/mol for the Peroxo, and Superoxo(s) clusters, respectively (**Figure 2).** As the consequence the PdO_2 superoxo species is much more reactive than the PdO_2 peroxo species. In the case of PdO_2 superoxo, there is a triplet to singlet intersystem crossing after the C-H bond cleavage TS since the final product ≡Pd(O)(CH_3OH) has a singlet ground state. The reaction proceeds first on the triplet PES before reaching the ≡Pd(OOH)(CH_3) intermediate where the system can switch its multiplicity and continue on the singlet PES. Such a mechanism is termed two-state reactivity (TSR) by Shaik et al.[38] The spin crossing is possible because of the small difference in the energy of the two lowest spin states (23 kJ/mol). This is analogous to the of C-H dissociation promoted by the ≡Pd(O) species.[18]

The geometry of the intermediates is given in **Figure S2** and that of the TSs in **Figure 3**. The main distances and angles are collected in **Table S4**. The C-H bond is highly stretched for the superoxo TS_1 (162-163 pm), but less for the peroxo (129 pm) (**Figure 3**). For comparison, this stretch is in the range obtained with other metal MO_2 (M: Fe (131pm) [20] and Mo (121 pm).[23] In a parallel way, the distance between O and H is longer for the peroxo TS (115 pm) than for the superoxo (104-107 pm). The structures of the superoxo TS_1 in triplet and singlet states are both not linear with an O1–O2– H angle of ∼104°.

Finally, the methanol formation over PdO_2 results in the formation of the oxygenated PdO oxo species that we have previously studied as the reactive center for methane oxidation to methanol.[18] Based on those previous results,[18] the desorption of methanol is endothermic on ≡Pd$(O)_{(t)}$(CH_3OH) by 50 kJ/mol.

3.3 Oxidation of methanol to formaldehyde on the ≡Pd(O) cluster

For the subsequent oxidation of methanol to formaldehyde by ≡Pd(O) according to reaction (Eq 4), we considered three possible reactions labeled Paths A, B and C and reported in **Scheme1.**

$$\equiv Pd(O)(CH_3OH) \rightarrow \equiv Pd\,(CH_2O)(H_2O) \qquad (4)$$

The first possibility is the C-H bond breaking as initial step (*Path A*). A second possibility is O-H bond breaking (*Path B)* and the third is the insertion of the C-O bond of methanol into the Pd-O_{oxo} bond (*Path C)*. In those mechanisms, formally two electrons are transferred to Pd, reducing Pd^{IV} into Pd^{II}. We considered both the singlet and triplet state potential energy surface since the reactant has a triplet ground state while the product is singlet. A summary of

the calculated reaction energy diagrams, considering the different paths is shown in **Figure 4**. The geometry of the intermediates is given in **Figure S3** and that of the TSs in **Figure 5** and the corresponding geometrical data in **Table s5a-S5b.**

First, path A starts with the H atom abstraction to form the $^{\bullet}CH_2OH$ radical, via the transition state TS_{3A} which produces directly the methanediol $\equiv Pd(CH_2(OH)_2$ as confirmed by IRC calculations. Starting on the triplet potential energy surface, this reaction step is strongly favored thermodynamically (ΔE = -208 kJ/mol) and shows very low activation energy ($\Delta E^{\ddagger}$ = 16 kJ/mol). Since $Pd(CH_2(OH)_2)$ has a singlet ground state, the system will switch to the singlet potential energy surface with a gain in energy of 82 kJ/mol. In a second step, this diol is dehydrated yielding $\equiv Pd(H_2O)(CH_2O)$ via a four-centered transition state $\mathbf{TS_{4A}}$. This step is slightly endothermic (ΔE = 12 kJ/mol) and has a rather high activation energy ($\Delta E^{\ddagger}$ = 135 kJ/mol).

Path B starts with the abstraction of the hydroxyl hydrogen of methanol (TS_{3B}) with a relatively small barrier of 44 kJ/mol on the triplet potential energy surface. This results in the formation of a first intermediate $\equiv Pd(OH)(CH_3O)^{I}$. The second step is the abstraction of a methylic H via TS_{4B} to form the formaldehyde and water on the surface. To access this TS, a reorientation of the methoxy group leading to the second intermediate $\equiv Pd(OH)(CH_3O)^{II}$ is necessary to ensure the formation of the H-O bond and facilitates the formation of water. This reorientation is quasi energy-neutral on the triplet potential energy surface (ΔE=-9k J/mol). The gap between the two spin states is strongly reduced at the stage of the reaction, the two reaction profiles being almost super-imposed (black and red paths in **Figure 4**). Then, the abstraction of the methylic hydrogen is almost barrier-less on both potential energy surfaces. Finally, the system switches to the singlet potential energy surface in the product. The rate-determining step of this path B is the initial O-H bond dissociation with a barrier of 44 kJ/mol.

The third alternative we considered (Path C) initiates with the insertion of the C-O bond of methanol into the Pd^{IV}-O_1 bond and occurs via a kind of metathesis mechanism. The methyl group coordinates to the O_1 atom and the OH group binds to Pd in a concerted manner via a four-centered transition state TS_{3C}, giving the hydroxyl intermediate, $\equiv Pd(OH)(CH_3O)^{III}$. The structure of this intermediate is shown on **Figure S3** that of the first TS is given on **Figure 5** and the corresponding geometrical data gathered in **Table S6**. The intermediate product is

stable by 22 kJ/mol with respect to the reactants complex, but the high barrier of 274 kJ/mol prevents path C from being reasonable. The next step is a proton transfer from the methoxy ligand to the hydroxyl ligand accompanied by the breaking of the Pd-O bond, via a five-centered transition state TS_{4C} with a small barrier ($\Delta E^{\ddagger}$ = 5 kJ/mol).

We conclude that the most likely mechanism is Path B, which start with the scission of the O-H bond of methanol. The corresponding transition state (TS_{3B}) is a rather late transition state with an already short O_1-H bond (105 pm) and a long O_2-H bond (142 pm) as represented in **Figure 5**. This transition state has geometrical characteristics similar to the CH activation one (TS_{3A}) and to the ones of the C-H activation on CH_4 by ≡Pd(O) on the triplet state. [18] While the OH scission is slightly more difficult that the CH one ($\Delta E^{\ddagger}$ = 44kJ/mol vs. 16 kJ/mol), Path A is clearly hampered by the stability of the diol intermediate ≡Pd($CH_2(OH)_2$. However, Baerends et al.[39] have studied the mechanism of methanol oxidation to formaldehyde by ($[Fe^{IV}=O]^{2+}$) and proposed that the reaction pathway involves the attack of the oxo oxygen at the C-H bond (Path A, in this work). The presence of the water ligands around the iron center clearly modifies the possible routes. On their side, Fellahet al. [21,22] have considered only the proton transfer from the OH of MeOH to form a methoxy species for the oxidation of methanol by N_2O on the $[Fe]^{1+}$-ZSM-5 cluster or on the $[VO]^{1+}$–ZSM-5 cluster. In a nutshell, we have shown that a single site palladium oxide species on Al-silica allows an easy methanol oxidation to formaldehyde. This has led us to investigate also the catalytic oxidation of methanol to formaldehyde by the superoxo species ≡Pd(O_2).

3.4 Oxidation of methanol to formaldehyde on the ≡Pd(O_2) Superoxo cluster

For the oxidation of methanol to formaldehyde by ≡Pd(O_2) according to reaction (Eq 5), only the triplet potential energy surface was investigated since it is the ground state of both the reactant ≡Pd(O_2) and final product ≡Pd(O).

$$\equiv Pd(O_2)(CH_3OH) \rightarrow \equiv Pd(O)(CH_2O)(H_2O) \qquad (5)$$

The energetic profiles are shown in **Figure 6**, the geometry of the intermediates is given in **Figure S4**, and that of the TSs in **Figure 7**. The corresponding geometrical data are gathered in **Tables S6-S9.**

The adsorption of methanol to the superoxo ≡Pd(O_2) leads to ≡Pd(O_2)(CH_3OH) with an exothermic reaction energy (ΔE = -12 kJ/mol, **Table 1**). In the adsorbed configuration, the Pd

atom interacts with four oxygen atoms including two oxygen atoms of the ring, the oxygen atom of methanol and one forming the superoxo species. This ML_4 type complex is approximately planar. A short hydrogen bond (166 pm, **Figure S4**) is formed between methanol and one oxygen of the ring. The corresponding H (H2) is easily captured by the framework oxygen atom in the first step, concomitantly with the methyl hydrogen (H1) abstraction by the superoxo. In the transition state (TS_5 in **Figure 7**), the incipient formation of the CH_2O is visible since, at the same time, the hydroxyl H is closer to the framework oxygen (OSi≡) than to the methanol oxygen (101 pm vs. 161 pm, **Table S6**) and the H of the CH_3 group is closer to the peroxo (117 pm vs. 141 pm). The distance that obviously changes the most is Pd-O3 (208 vs. 266 pm, **Table S6**) between Pd and the formaldehyde oxygen. The hydrogen atom has been completely transferred to OSi≡ in the resulting intermediate. This reaction step is slightly endothermic (ΔE = 8 kJ/mol) and shows an accessible activation barrier of $\Delta E^{\ddagger}$ = 80 kJ/mol, suggesting that framework oxygen atoms can be involved directly in the methanol activation. Several studies have shown that the framework oxygen atoms are worth being considered in H-abstraction from small hydrocarbons. [15,40-44] In addition, a recent work suggests that Lewis acid sites may activate C–H and O–H bond activation in methanol.[45] Ma et al.[16] have reported in their theoretical study that the first step is the formation of methanediol on the superoxo species $[PdO_2]^{2+}$ grafted in the 6-membered ring. The difference with the results presented here is probably due to the interaction between the H atom of methanol and the framework oxygen atoms, which varies from a 6-membered ring to an 8-membered ring (this study). In other words, the reactivity of Pd^{II} superoxo sites depends on their local geometrical environment.

This synchronous abstraction of a methyl hydrogen atom (H1) and a proton (H2) transfer to one oxygen atom of the ring generates the intermediate ≡Pd(OOH)(CH_2O)(H)OSi≡ (**Figure S4**). From this intermediate, several possibilities were considered. Firstly, the formaldehyde formed on the cluster can easily desorb from the surface to lead to the intermediate ≡Pd(OOH)(H)OSi≡, with a desorption energy of 31 kJ/mol (**Figure 6**). Based on the fact that protons in zeolites are known to be mobile, [40,44] one framework oxygen atom adjacent to the Al could accept the proton (H)OSi≡ to form a Brønsted acid site (H)OAl≡. The transfer of the proton generates the intermediate ≡Pd(OOH)(H)OAl≡ (**Figure S5).** This exothermic reaction step (ΔE = -90 kJ/mol, **Figure 6**) is barrier less. The subsequent last step is the decomposition of the oxyhydroxide PdOOH and the formation of water. In the corresponding transition state **TS_6**, the proton is transferred from the framework oxygen (O-Al) to the hydroxyl oxygen of

PdOOH (O_2 in **Figure 7**) and at the same time, the O−OH bond is broken, resulting in H_2O formation adsorbed on the $[PdO]^{2+}$ active site. The activation energy of this process is very high (200 kJ/mol, **Figure 6**). Hence, from the height of this barrier, it is already clear that this pathway is very unlikely.

If no desorption occurs, a very stable methanediol intermediate can be obtained via the three centered transition state TS_7 (**Figure 6** and **Table S8**). The proton transfer from the framework oxygen atom (O-Si) to O of formaldehyde and, at the same time the OH transfer from PdOOH moiety to carbone of the formaldehyde happen, leading to the methanediol adsorbed on ≡Pd(O), labeled ≡Pd(O)($CH_2(OH)_2$). IRC calculations have confirmed this connection. This exothermic reaction step (ΔE = -110 kJ/mol, **Figure 6**) occurs with a barrier of 90 kJ/mol. The methanediol product is very stable thermally, but can be converted to adsorbed water and formaldehyde via a three-centered transition state **TS_8** (**Figure 7** and **Table S9**) whose structure is similar to TS_{4A}. The chemical equilibrium between formaldehyde and methanediol, is dominantly shifted in favor of formaldehyde in the gas phase (ΔE = -7 kJ/mol, **Figure 6**) in agreement with other theoretical work.[46] The barrier that we have found is very high (188 kJ/mol, **Figure 6**), therefore, it is already clear that this pathway is very improbable. This value is very close to the theoretical value of 187kJ/mol for the decomposition of methanediol to formaldehyde in the gas phase,[46] showing that this step is barely catalyzed in our case.

Another alternative reaction path for the decomposition of methanediol can be also propose. It starts with of the transfer of hydrogen (H1) from methanediol transfer to PdO1 concomitant with a homolytic splitting of the C-O3 bond, which results in formaldehyde adsorbed on palladium(II) hydroxide $Pd(OH)_2$. The geometry of the corresponding five-centered transition state TS_9 is shown in **Figure 7**. This reaction is an endothermic step (ΔE = +8 kJ/mol,) with an activation barrier value of 90 kJ/mol. After, the formaldehyde desorbs with a desorption barrier of 40 kJ/mol. The next reaction is the formation of water from ≡$Pd(OH)_2$ cluster via a three-centered transition state TS_{10} (**Figure 6** and **Table S8**). For this step, the proton (H1) transfer from one OH group to the other one with, at the same time, a homolytic Pd–O3 bond cleavage results in the formation of adsorbed water, the final product being labeled ≡Pd(O)(H_2O) (**Figure S4**). This reaction step is exothermic (ΔE = -23 kJ/mol, Figure 6) and shows a low activation barrier ($\Delta E^{\neq}$ = 36 kJ/mol, **Figure 6**). Provided the relatively low height of those activation barriers, the following mechanism is the most likely to oxidize

methanol into formaldehyde on ≡Pd(O_2). It is consist in four steps: (i) Generation of formaldehyde by a synchronous transfer (TS5) yielding ≡Pd(OOH)(CH_2O)(H)OSi≡ (ii) Proton transfer from (H)OSi≡ and OH transfer from PdOOH to form methanediol (TS7) (iii) Formation of formaldehyde and Pd$(OH)_2$ moiety (TS9) (iv) Dehydration of Pd$(OH)_2$ (TS10). The limiting step is either the second step either the third step with barriers of 90/89 kJ/mol.

4. Discussion

In this theoretical study, we investigated the full catalytic cycle of the oxidation of methane to formaldehyde by molecular O_2 catalyzed by Pd deposited on aluminosilicate 8-MR. The catalytic site has been identified as an isolated Pd^{2+} coordinated by basic oxygens of the alumino-silicate network, noted ≡Pd in this article and represented in **Figure S1**. To be active towards methane oxidation, this site needs first to be oxidized into Pd(IV) under its oxo form (≡Pd(O)). This raises the question of the generation/regeneration of this catalytic site. The catalytic cycle starts with the adsorption of molecular O_2 resulting in the formation of $[PdO]^{2+}$ or /and $[PdO_2]^{2+}$ sites, respectively. The formation of ≡Pd(O) site has been investigated on the same cluster models and discussed in our previous theoretical studies.[25] The oxidation of ≡Pd to ≡Pd(O) is found endothermic while the oxidation to ≡Pd$(O_2)_{superoxo(t)}$ is an exothermic reaction ((ΔE=-48kJ/mol, **Table 1**), which shows that the catalytic cycle starts by the formation of ≡Pd(O_2). The general picture is that O_2 interacts on the reduced Pd site and participates in the oxidation of methane or methanol, restoring the ≡Pd(O) structure, as it is also known experimentally.[47] This leaves the opportunity for competition between the two sites PdO and PdO_2 with the two reactants as shown in the cycle represented in **Scheme 2**. Based on the results part, we selected here the best reaction pathway for each branch of the cycle, namely methane oxidation to methanol over the ≡Pd(O) and methanol to formaldehyde over the ≡Pd(O_2) site in silica, and gathered the corresponding reaction profiles in **Figure 8.** Activation barriers and desorption energies for the respective reaction steps involved in the global reaction of methane oxidation to formaldehyde are tabulated in **Table 1**.

Let's start considering the oxidation of methane. The two sites behave in a similar way. Typically, the cleavage of a C−H bond (TS_1) is the important initial step as shown in the profiles in **Figure 8**. The activation barrier for this hydrogen abstraction from CH_4 to ≡Pd(O_2) and ≡Pd(O) clusters are 152 and 90 kJ/mol, respectively. This shows that the Pd oxo species supported on Al-MCM-41 silica catalyst is more active than the Pd superoxo species for methane oxidation. Previous experimental[47] and theoretical[48] studies reporting that the catalytic surface PdO(111) site is more active than surface PdO_2(111) in the oxidation of CH_4

support that conclusion. A similar finding has been reported previously for the activation barrier of the C–H bond scission by Fe catalysts: the FeO oxo[49] species (50 kJ/mol) is more active than the (FeO_2) Dioxo and Peroxo species[23] (70 and 151 kJ/mol, respectively). If methanol desorbs from the surface, desorption energies values are 14 kJ/mol for ≡Pd(O_2) and 49[18] kJ/mol for ≡Pd(O).

As far as the methanol oxidation is concerned, the proposed mechanisms on the two sites are different. In the case of ≡Pd(O), the first step is the dissociation of the O–H bond and methoxy formation (TS_{3B}), followed by an easy C-H scission (TS_{4B}) leading to formaldehyde. This process is rather smooth energetically. The limiting step is the first one with a barrier of 44kJ/mol. On ≡Pd$(O_2)_{superoxo}$, both C–H and O–H bonds of methanol dissociate simultaneously yielding formaldehyde, adsorbed on a ≡Pd(OOH) cluster (TS5). This step is promoted by the active participation of one oxygen atom of the silicate framework ≡SiO that becomes protonated. It is worthy noting that the direct dehydrogenation of methanol with two framework oxygen atoms ≡SiO is less effective than having one of the framework oxygen ≡SiO and one of oxygen of ≡Pd$(O_2)_{superoxo}$, comparing a highest barrier of 243 kJ/mol[50] to 90 kJ/mol. This combination acts as an acid/base pair. Then, the methanediol is formed through another synchronous step: ≡SiOH transfers back a proton to the formaldehyde oxygen while the hydroxyl migrates from the Pd center to the formaldehyde carbon (TS7). This step is the most demanding energetically along this path ($\Delta E^{\ddagger}$ = 90 kJ/mol) that continues with the generation of formaldehyde, water and the ≡Pd(O) site. A direct comparison of the energetic profiles corresponding to the two sites in **Figure 8** shows that here again, ≡Pd(O) is much more active than ≡Pd(O_2). This conclusion is also supported by an experimental study Wojcieszak et al,[51] which reports that the first reaction step would be the formation of methoxy groups by dissociative adsorption of methanol and then their transformation into formaldehyde. The formation of intermediate methanediol species has not been detected experimentally, which confirmed our findings.

After these reactions, water and formaldehyde formed on the clusters will desorb from the surfaces to complete the catalytic cycle. Those desorption are endothermic but not too demanding energetically (see **Table 1**). Hence, they will be easily overcome entropically thanks to temperature and allow the regeneration of the active site (see **Table S1**).

In a nutshell, for the oxidation of both methane and methanol, the oxo species is more active than the superoxo species. Moreover, methanol is more easily oxidized than methane, with barriers that are systematically lower by ~40 to 50 kJ/mol.

Scheme 2 sketches the complete catalytic cycle of the transformation showing two elementary cycles. The corresponding energy profiles are shown in **Figure 9**. In the top cycle (corresponding profile shown in black), the methane oxidation into methanol is performed by ≡Pd(O_2) with a high barrier of 152 kJ/mol (TS1), yielding to ≡Pd(O) and methanol that easily further react to regenerate the active site Pd^{2+} and formaldehyde and water. In this cycle, the key step is the initiation of the reaction. As written above, at the beginning of the reaction, the present species must be ≡Pd(O_2) and methane and this cycle corresponds to this initiation stage. However, further in the catalytic bed, once methanol is formed, methanol can react with ≡Pd(O_2) in a relatively easy way, leading to formaldehyde and generating ≡Pd(O). This latter species acts then as a new catalyst, more active in methane oxidation. This opens a second cycle (bottom one in **Scheme 2**, corresponding energy profile in red in **Figure 9**) that is much more efficient than the initiation one as clearly shown by the superposition of the corresponding energy profiles in **Figure 9**. The black profile has higher transition states and lower intermediates than the red one. To facilitate the switch to the most efficient cycle, we suggest adding a small amount of methanol in the feed. This could allow a lower temperature for the reaction to proceed.

5. Conclusion

Density functional theory (DFT) calculations were carried out in a study of the oxidation of methane to formaldehyde occurring on Pd(II)/Al-MCM-41. Two mechanisms have been proposed, the first one is based on the assumption that the active centers are Pd-Oxo species, whereas the second mechanism assumes that the active centers are PdO_2-Superoxo species. In addition, we have investigated the competition of methane / methanol substrates on active sites. An important finding of the present work is that for the oxidation of both methane and methanol, the oxo species is more active than the superoxo species. Then, raises the question of the regeneration of this very active center. O_2 can adsorb on Pd^{2+} yielding a PdO_2-Superoxo species. In this species, the O=O bond cannot be easily split. However, if used as an active center to oxidize either methane or methanol, this species is turned into a Pd-Oxo species, closing the catalytic cycle. This regeneration is better performed in presence of methanol.

Conflicts of interest

The authors declare no competing financial interest.

Acknowledgements

The authors would like to acknowledge the financial support of the Tunisian General Direction of Scientific Research and Technological Renovation (DGRSRT) and the Institut Français de Tunisie. Grants of computer time from the Pole of Numerical Simulations (PSMN), Ecole Normale Supérieure de Lyon, are gratefully acknowledged.

References

1 D. Cheng, K. Okumura, Y. Xie and C.-J. Liu, Appl. Surf. Sci., 2007, **254**, 1506–1510.

2 B.Yue, R. Zhou, Y. Wang and X. Zheng, Appl. Surf. Sci., 2006, **252**, 5820–5828.

3 K. Persson, L.D. Pfrefferle, W. Schwartz, A.Ersson and S.G. Järås, Appl. Catal. B, 2007, **74**, 242–250.

4 C.-J. Liu, K. Yu, Y.-P. Zhang, X. Zhu, F. He and B. Eliassion, Appl. Catal. B 2004, **47** 95–100.

5 R. Burch, D.J. Crittle and M.J. Hayes, Catal. Today 1999, **47**, 229–234.

6 P. Gélin and M. Primet, Appl. Catal. B, 2002, **39**, 1–37.

7 J.R. Paredes, E. Díaz, F.V. Díez and S. Ordónez, Energy Fuels, 2009, **23**, 86–93.

8 A. Gannouni, B.Albela, M. Saïd Zina and L. Bonneviot, Appl. Catal. A, 2013, **464**, 116–127.

9 F.Yin, S. Ji, P. Wu, F. Zhao and C. Li, J. Catal., 2008, **257**, 108–116.

10 J.-H. Park, B. Kim, C.-H. Shin, G. Seo, S.H. Kim and S.B. Hong, Top. Catal., 2009, **52**, 27–34.

11 K. Okumura, E. Shinohara and M. Niwa, Catal. Today, 2006, **117**, 577–583.

12 A.Gannouni, S. Zribi, R. Dardouri and Z. Saïd, J. Tun. Chem. Soc., 2017, **19**, 115–123.

13 K. Okumura,; S. Masumoto, N. Nishiaki and M. Niwa, Appl. Catal. B, 2003, **40**,151–159.

14 J. Bassil, A. AlBarazi, P. Da Costa and M. Boutros, Catal. Today, 2011, **176**, 36–40.

15 Y. Lou, J. Ma, W.D. Hu, Q.G. Dai, L. Wang, W.C. Zhan, Y.L. Guo, X.M. Cao, Y. Guo, P.J. Hu and G.Z. Lu, ACS Catal., 2016, **6**, 8127–8139.

16 Y. Shen, Q. Meng, S. Huang, J. Gong and X. Ma, Phys.Chem. Chem. Phys., 2013,**15**, 13116−13127.

17 P. Begum and R.C. Deka, Chemistry Select 2017, **2**, 8847–8855

18 A. Gannouni, F. Delbecq, M. Saïd Zina, P. Sautet, J. Phys. Chem. A, 2017, **121**, 5500–5508.

19 J.G. Wang and C.J. Liu,. J. Mol. Catal. A: Chem., 2006, **247**, 199–205.

20 S. Chempath and A.T. Bell, J. Catal., 2007, **247**, 119–126.

21 M. Ferdi Fellah, J. Catal., 2011, **282**, 191–200.

22 M. Ferdi Fellah, and I. Onal, *Phys.Chem. Chem. Phys.,* 2013, **15**, 13969–13977.

23 W.Z. Liang, A. T. Bell, M. Head-Gordon and A.K. Chakraborty, J. Phys. Chem. B, 2004, **108**, 4362-4368.

24 M. Ferdi Fellah, and I. Onal, *J*. Phys. Chem. C, 2010, **114**, 3042–3051.

25 A. Gannouni, X. Rozanska, B. Albela; M.Saïd Zina, F.Delbecq, L.Bonneviot and A. Ghorbel, J. Catal., 2012, **289**, 227–237.

26 J.Sauer, P. Ugliengo, E.Garrone and V.R. Saunders, Chem. Rev., 1994, **94**, 2095–2160.

27 J. Sauer and J.R. Hill, Phys. Lett. 1994, **218**, 333–337.

28 M.A. Zwijnenburg, S.T. Bromley, J.C. Janses and T. Maschmeyer, Chem. Mat. 2004, **16**, 12–20.

29 C. S. Guo, K. Hermann, M. Hävecker, A. Trunschke and R. Schlögl, J. Phys. Chem. C 2012, **116**, 22449−22457

30 C. R. Landis, C. M. Morales, S. S. Stahl, J. Am. Chem. Soc. 2004, **126**, 16302–16303.

31 B. V. Popp, C. M. Morales, C. R. Landis and S. S. Stahl,. Inorg. Chem 2010, **49**, 8200–8207.

32 M. J. Frisch, G. W.Trucks, H. B. Schlegel, G. E. Scuseria, M. A. Robb, J. R. Cheeseman, G. Scalmani, V. Barone, B. Mennucci, G. A. Petersson, and al. Gaussian 09, Revision D.01; Gaussian, Inc.: Wallingford, CT, 2009.

33 N. C. Handy and A. J. Cohen, Mol. Phys., 2001, **99**, 403−412.

34 A. R.Groenhof, M. Swart, A. W. Ehlers and K. Lammertsma. J. Phys. Chem., A, 2005, **109**, 3411−3417.

35 P. C. Andrikopoulos, C. Michel, S. Chouzier and P. Sautet, ACS Catal., 2015, **5**, 2490−2499.

36 A. Schäfer, C. Huber and R. Ahlrichs, J. Chem. Phys., 1994, **100**, 5829−5835.

37 R.S. Mulliken, J. Chem. Phys., 1955, **23**, 1833−1840.

38 D.Schröder, S. Shaik, H. Schwarz, Acc. Chem. Res., 2000, **33**, 139−145.

39M. J. Louwerse, P. Vassilev and E. J. Baerends, J. Phys. Chem. A, 2008, **112**, 1000−1012.

40 V. L. Sushkevich1, D. Palagin1, M. Ranocchiari and J.A. van Bokhoven, Science, 2017, **356**, 523−527.

41S. Wannakao, C. Warakulwit, K. Kongpatpanich, M. Probst and J. Limtrakul, ACS Catal., 2012, **2**, 986−992.

42 B. Ding, S. Huang and W. Wang, Appl. Surf. Sci., 2008, **254**, 4944−4948.

43 M. Rutigliano, N. Sanna and A. Palma, Computational and Theoretical Chemistry, 2015, **1074**, 9–18.

44 J. A. Ryder, A. K. Chakraborty and A. T. Bell, J. Phys. Chem. B, 2000, **104**, 6998–7011.

45 B. C. Bukowski and J. Greeley, J. Phys. Chem. C, 2016, **120**, 6714−6722.

46 M. Kumar, J. M. Anglada and J. S. Francisco, J. Phys. Chem. A 2017, **121**, 4318−4325.

47 F. Yin, S. Ji, P. Wu and F. Zhao, J.Catal., 2008, **257**, 108–116.

48 Y. H.Chin, C. Buda, M. Neurock and E Iglesia, J. Am. Chem. Soc., 2013, **135**, 15425–15442.

49 A. L.Yakovlev, G. M. Zhidomirov and R. A. van Santen, J. Phys. Chem. B, 2001, **105**, 12297–12302.

50 P. N. Plessow and F. Studt, ACS Catal., 2017, **7**, 7987–7994.

51 R. Wojcieszak, A. Karelovic, E. M. Gaigneaux and P. Ruiz, Catal. Sci. Technol., 2014, **4**, 3298–3305.

Table 1 Relative Energies ΔE (kJ/mol), Activation Energies $\Delta E^{\ddagger}$ (kJ/mol) and Imaginary Frequencies (cm^{-1}) for each transition state for direct oxidation of methane to formaldehyde on ≡Pd(O_2) and on ≡Pd(O) clusters. All species are in their triplet ground state except ≡Pd(s) that is in its singlet ground sate.

Reaction	Steps	≡Pd(O_2)	≡Pd(O)
		ΔE / $\Delta E^{\ddagger}$ / Freq	**ΔE / $\Delta E^{\ddagger}$ / Freq**
≡Pd(s) → ≡Pd(t)	Spin flip		72
≡Pd + O_2 → ≡Pd(O_2)			-10
≡Pd(O) + ½ O_2 → ≡Pd(O_2)	Adsorption of molecular O_2		-48
≡Pd + ½ O_2 → ≡Pd(O)			38
≡Pd(O_2) + CH_4 → ≡Pd(O_2) (CH_4)	Methane adsorption	0.51	-0.9[a]
≡Pd(O) + CH_4 → ≡Pd(O) (CH_4)			
≡Pd(O_2) (CH_4) → ≡Pd(OOH)(CH_3)	**TS1:** Proton transfer from the CH_4 to form radical methyl	149 / 152 / 454i	53 / 90 / 734i [a]
≡Pd(O) (CH_4) → ≡Pd(OH) (CH_3)			
≡Pd(OOH)(CH_3) → ≡Pd(O)(CH_3OH)	**TS2:** Hydroxyl transfer from the active species to form methanol	-195 / 60 / 632i	-234 / 7 / 123i [a]
≡Pd(OH)(CH_3) → ≡Pd (CH_3OH)			
≡Pd(O)(CH_3OH) → ≡Pd(O) +CH_3OH	Desorption of methanol	14	49[a]
≡Pd(CH_3OH) → ≡Pd +CH_3OH			
≡Pd(O_2) + CH_3OH → ≡Pd(O_2)(CH_3OH)	Adsorption of methanol	-12	-14
≡Pd(O) + (CH_3OH) → ≡Pd(O)(CH_3OH)			
≡Pd(O)(CH_3OH) → ≡Pd(OH)(CH_3O)	**TS3**: Proton transfer from the OH to form methoxy		6 / 44 / 388i
≡Pd(OH)(CH_3O) → ≡Pd(H_2O)(CH_2O)	**TS4**: Proton transfer from the methoxy to form formaldehyde and water		-225 / 2 / 578i
≡Pd(O_2) (CH_3OH) → ≡Pd(OOH)(CH_2O) (H)OSi≡	**TS5**: Proton transfer from the carbon atom to form active species	8 / 80 / 987i	
≡Pd(OOH)(CH_2O) (H)OSi≡ → ≡Pd(O)($CH_2(OH)_2$)	**TS7:** Proton transfer from O_{MS} and OH transfer from PdOOH to form methanediol	-110 / 90 / 520i	
≡Pd(O)($CH_2(OH)_2$) → ≡Pd($OH)_2$(CH_2O)	**TS9:** Formation of formaldehyde	8 / 89 / 1254i	
≡Pd($OH)_2$(CH_2O) → ≡Pd($OH)_2$ + CH_2O	Desorption of formaldehyde	40	19
≡Pd(H_2O)(CH_2O) → ≡Pd(H_2O) + CH_2O			
≡Pd($OH)_2$ → ≡Pd(O)(H_2O)	**TS10:** Formation of water	-23 / 36 / 1456i	
≡Pd(O)(H_2O) → ≡Pd(O)+(H_2O)	Desorption of water	10	47
≡Pd(H_2O) → ≡Pd + H_2O			

[a] Gannouni et al. [22] The Pd^{2+} oxo species supported on a 8-membered ring

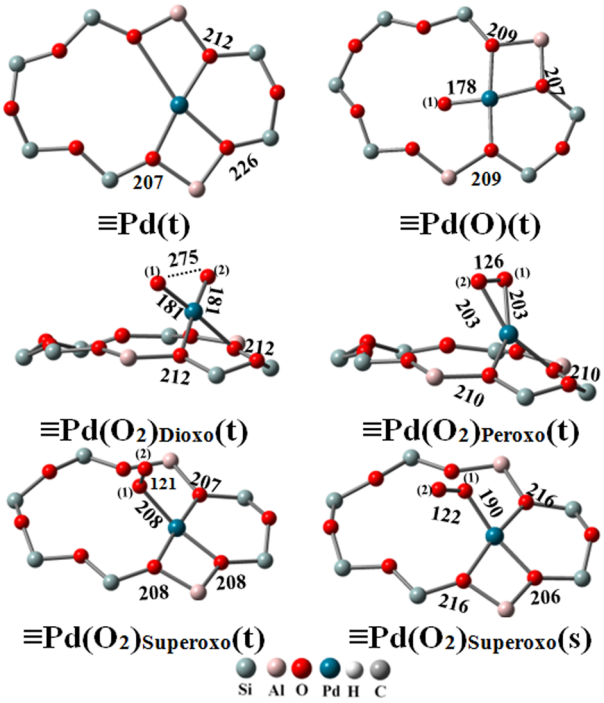

Fig. 1 UOPBE/TZVP-optimized geometries of ≡Pd ; ≡Pd(O) ; ≡$Pd(O_2)_{Dioxo}$; ≡$Pd(O_2)_{Peroxo}$; ≡$Pd(O_2)_{Superoxo}$(t) and ≡$Pd(O_2)_{Superoxo}$(s). The bond lengths Pd-OMS in pm, and s and t in the parentheses indicate singlet and triplet, respectively. Pictures restricted to rings containing $[PdO_2]^{2+}$ species.

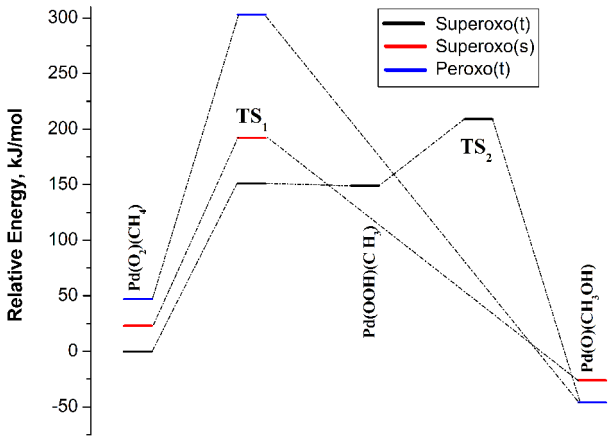

Fig. 2 Potential energy diagram for the ≡$Pd(O_2)$ + CH_4 → ≡Pd(O) + CH_3OH bond activation of methane on ≡$Pd(O_2)_{Peroxo\ (t)}$; ≡$Pd(O_2)_{Superoxo(t)}$ and ≡$Pd(O_2)_{Superoxo(s)}$, clusters calculated at the UOPBE level.

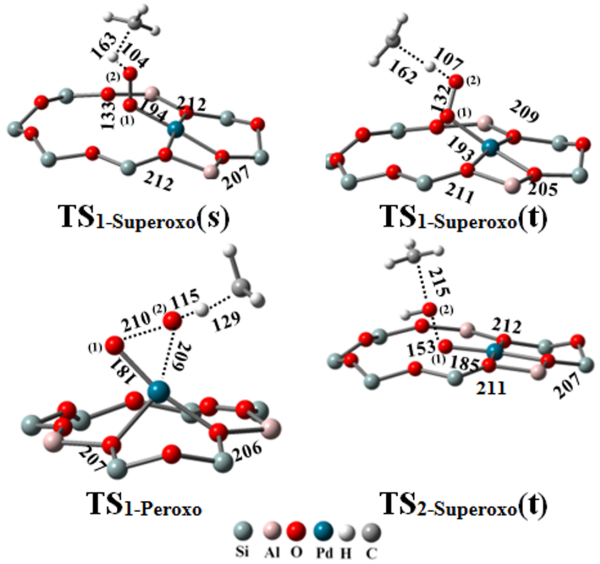

Fig. 3 UOPBE/TZVP-optimized geometries of the transition states of the reaction ≡Pd(O_2) + CH_4 → ≡Pd(O) + CH_3OH for different species as follows: Peroxo and superoxo. The bond lengths are given in pm, and s and t in parentheses indicate singlet and triplet, respectively.

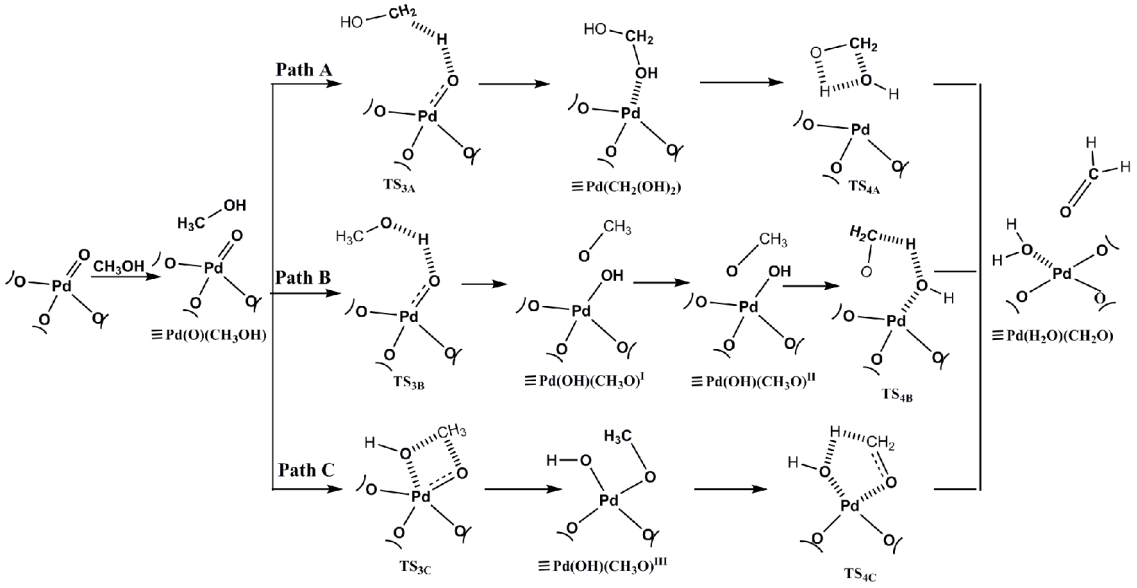

Scheme 1 Three possible reaction pathways for the oxidation of methanol to formaldehyde.

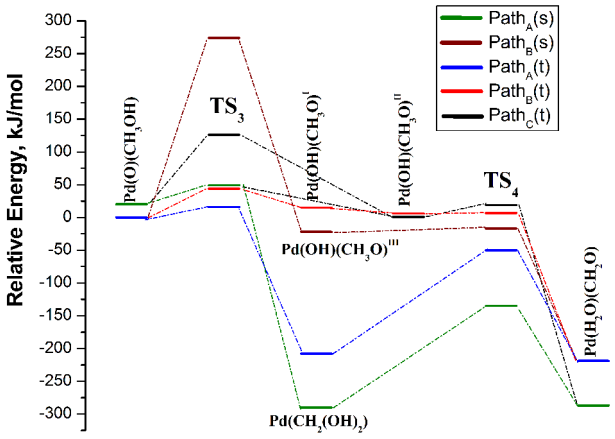

Fig. 4 Potential energy diagram for direct methanol oxidation to formaldehyde on the ≡Pd(O) cluster calculated at the UOPBE level.[2]

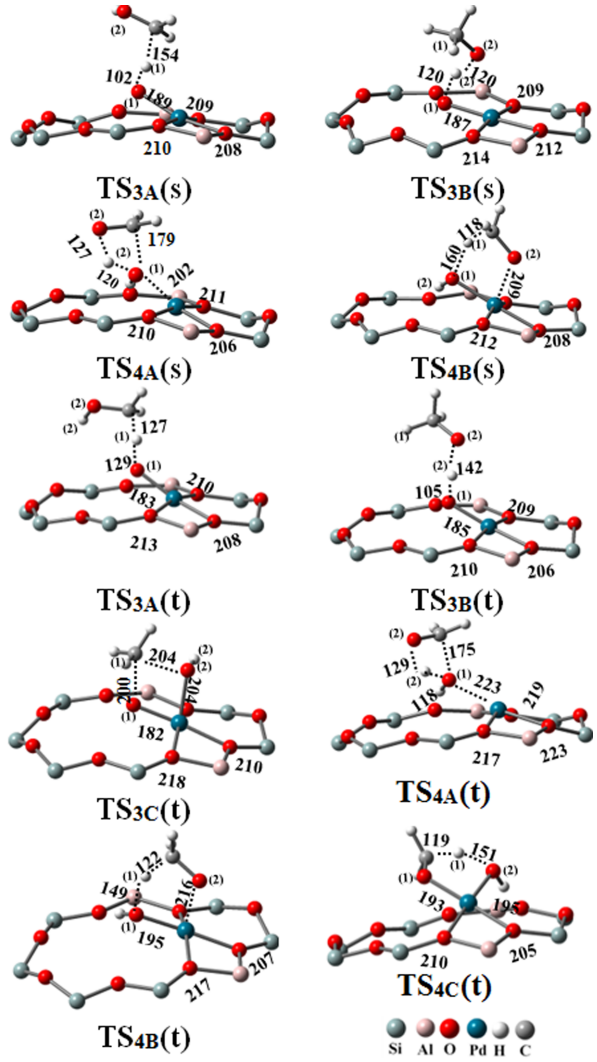

Fig. 5 UOPBE/TZVP-optimized geometries of the transition states for direct methanol oxidation to formaldehyde on the ≡Pd(O) cluster for different pathway. The bond lengths are given in pm, and s and t in parentheses indicate singlet and triplet, respectively.

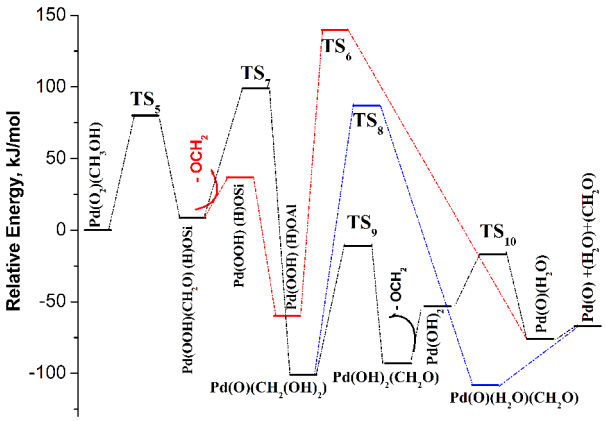

Fig.6 Potential energy diagram for direct methanol oxidation to formaldehyde on the ≡Pd(O_2) cluster calculated at the UOPBE level.

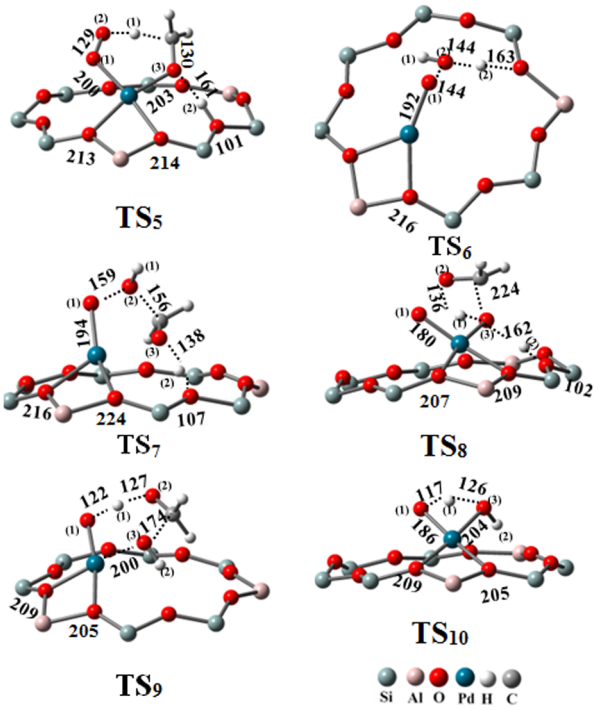

Fig. 7 UOPBE/TZVP-optimized geometries of the transition states for direct methanol oxidation to formaldehyde on the ≡Pd(O_2) cluster for different pathway. The bond lengths are given in pm.

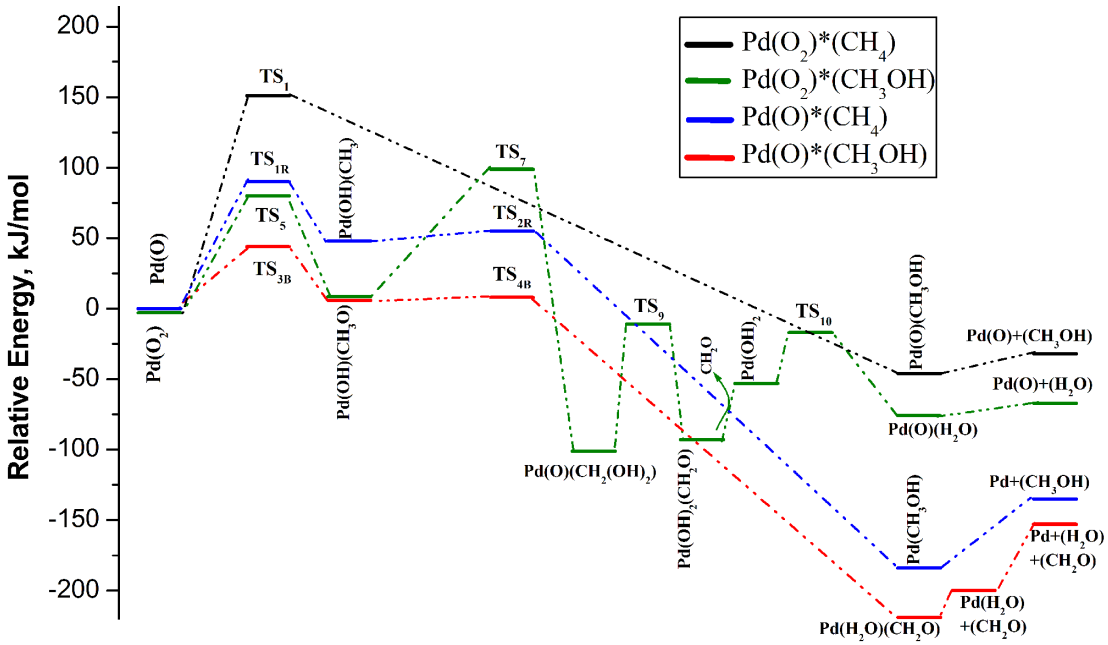

Fig. 8 Relative energy profile for direct methane oxidation to methanol and methanol to formaldehyde on ≡Pd(O_2) and on ≡Pd(O) clusters. Corresponding reaction energies, activation energies are shown in Table 1.

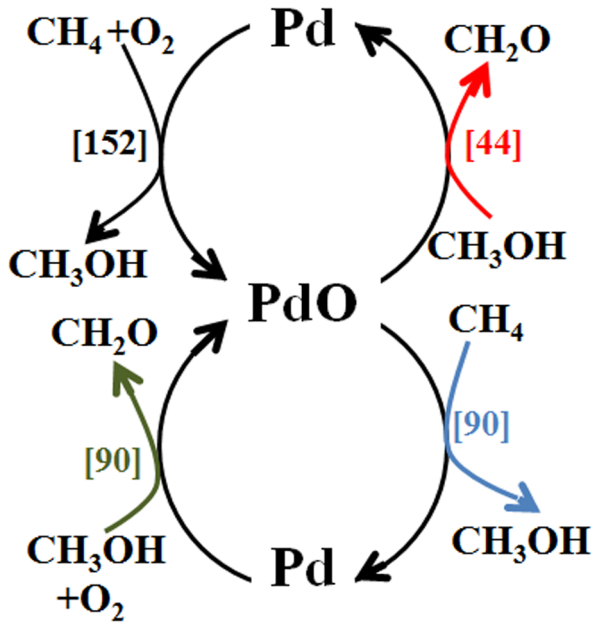

Scheme 2 Catalytic Cycle for the mechanism of methane oxidation to formaldehyde occurring on Pd(II)/Al-MCM-41. Activation Energies $\Delta E^{\ddagger}$ (kJ/mol) are presented in brackets [$\Delta E^{\ddagger}$].

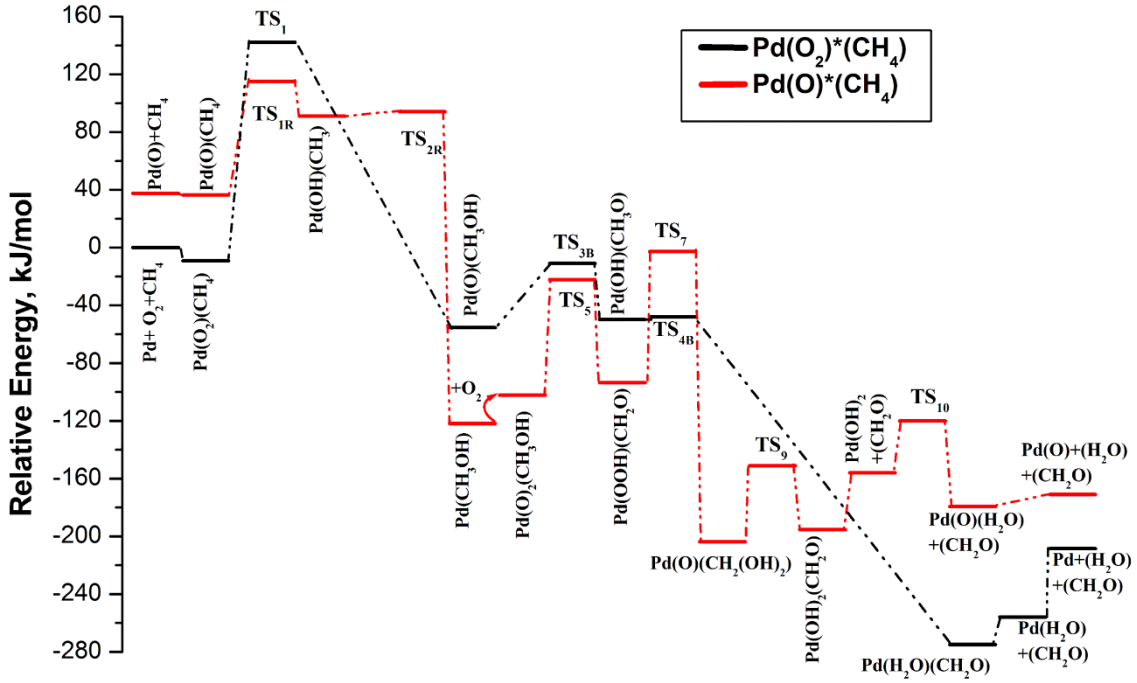

Fig. 9 Relative energy profile for direct methane oxidation to formaldehyde on [PdO_2] and [PdO] sites in Pd(II)/Al-MCM-41